RSC Advances

ROYAL SOCIETY OF CHEMISTRY

www.rsc.org/advances

TOC entry

A method to prepare oxide - carbon nanotube composite electrodes for lithium-ion batteries has been demonstrated. A phase with severe transport limitations, $LiFeTiO_4$, has been selected as a model electrode material.

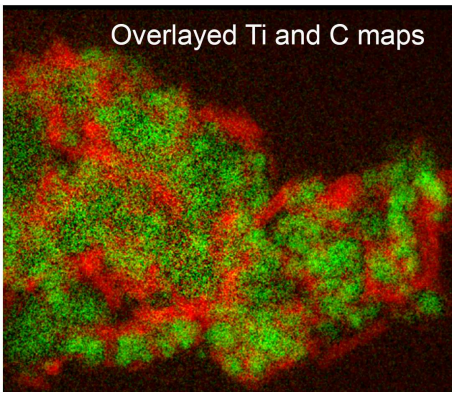

T. Tao, M. M. Rahman, T. Ramireddy, J. Sunarso, Y. Chen, A. M. Glushenkov*

Preparation of composite electrodes with carbon nanotubes for lithium-ion batteries by low-energy ball milling

Journal Name

RSCPublishing

ARTICLE

Preparation of composite electrodes with carbon nanotubes for lithium-ion batteries by low-energy ball milling

Cite this: DOI: 10.1039/x0xx00000x

Received 00th January 2012,
Accepted 00th January 2012

DOI: 10.1039/x0xx00000x

www.rsc.org/

T. Tao[a], M. M. Rahman[a], T. Ramireddy[a], J. Sunarso[b], Y. Chen[a] and A. M. Glushenkov[a,c]*

Some of the prospective electrode materials for lithium-ion batteries are known to have electronic transport limitations preventing them from being used in the electrodes directly. In many cases, however, these materials may become practical if they are applied in the form of nanocomposites with a carbon component, e.g. via incorporating nanoparticles of the phase of interest into a conducting network of carbon nanotubes. A simple way to prepare oxide-carbon nanotube composites suitable for the electrodes of lithium-ion batteries is presented in this paper. The method is based on low-energy ball milling. An electrochemically active but insulating phase of $LiFeTiO_4$ is used as a test material. It is demonstrated that the $LiFeTiO_4$ – carbon nanotube composite is not only capable of having significantly higher capacity (~105-120 mAh g^{-1} vs. the capacity of ~65-70 mAh g^{-1} for the $LiFeTiO_4$ nanoparticles) at a slow current rate but may also operate at reasonably high current rates.

1. Introduction

Commercial Li-ion batteries traditionally use $LiCoO_2$ as the cathode and graphite as the anode [1]. It is beneficial to replace these conventional materials with superior electrode materials in order to improve energy and power densities of the batteries as well as to increase the safety of lithium-ion devices [2, 3]. However, in many cases the prospective electrode materials have some transport limitations such as limited electronic and/or ionic conductivity. A well-known example is a cathode material $LiFePO_4$ [4, 5], which has faced some practical issues initially but is already commercialised. The transport limitations in this material can be neutralised via using this phase in the nanostructured form (to facilitate the ionic transport) and employing continuous carbon coating to provide the efficient supply of electrons [6, 7]. Similar approach works with other insulating phases and this area of research has been summarised in detail by Li and Zhou [8].

An alternative way to overcome the issue of limited electronic conductivity in the electrode materials is to use networks of carbon nanotubes that can be mixed with the active material to form nanocomposites [9-11]. This is particularly beneficial for situations where improvements in rate capability are required [10, 11]. The nanotubes act as conducting cables to provide electron transport from current collectors through the bulk of the electrode in an efficient manner. There are a few reported techniques to incorporate networks of nanotubes into the electrodes of Li-ion batteries. For example, hydrothermal method [12, 13], vacuum filtration method [14] and deposition in anodised alumina templates [15] have been employed. Some authors have also attempted to grow active electrode materials directly on carbon nanotubes [16].

In this paper, a simple method for the preparation of oxide – carbon nanotube composite electrodes is presented. The method is based on a low-energy ball milling treatment. $LiFeTiO_4$ is used as a test electrode material. This phase exhibits reversible electrochemical reactivity with lithium [17-20] but is known to have an insulating nature [18]. A theoretical capacity of 153.5 mAh g^{-1} has been suggested [18]. It can normally display only limited capacity even when used in the form of nanoparticles. We demonstrate that significant improvement is achieved when the composite of $LiFeTiO_4$ and MWCNTs is prepared by the suggested method and used as an electrode material. Considerably higher capacity is displayed by the composite electrode (~105-120 mAh g^{-1} instead of ~65-70 $mAhg^{-1}$ for the $LiFeTiO_4$ nanoparticles), and the electrode is capable of operating under relatively fast charge-discharge rates (currents of up to 500 mA g^{-1} were evaluated). The results indicate that the proposed method for preparing composite electrodes can indeed significantly improve the characteristics of the model electrode based on an insulating phase.

2. Experimental

2.1. Materials and synthesis: $LiOH{\cdot}H_2O$ (>98%, Sigma-Aldrich, 402974) and ilmenite powder ($FeTiO_3$, 99% purity; Consolidated Rutile Ltd, Australia) were used as starting materials for the preparation of $LiFeTiO_4$ nanoparticles. The nanoparticles were produced by a two-step procedure involving ball milling treatment and subsequent heating. 10 grams of a mixture of $FeTiO_3$ and $LiOH{\cdot}H_2O$ powders in a molar ratio of

1: 1 were loaded inside a stainless steel milling container together with four hardened steel balls (diameter of 25.4 mm). The mixture was milled in a magneto-ball mill (described in detail elsewhere [21]) at a rotation speed of 160 rpm for 150h at room temperature under Ar atmosphere of 100 kPa. The magnet was kept in a 45° position in order to cause the balls to provide strong impacts inside the mill. In the following heating process 1 g of the milled mixture of $FeTiO_3$ and $LiOH \cdot H_2O$ was loaded into an alumina combustion boat and the boat was placed into the centre of a horizontal tube furnace. The temperature in the furnace was raised from room temperature to 400 °C within about 30 min and kept at that level for 12 h. At the end of the heating procedure, the furnace was allowed to cool down to room temperature in argon gas flow. Argon gas flow (50 ml/min) was maintained though the furnace tube for the duration of the whole procedure. Commercially available multi-walled carbon nanotubes (MWCNTs) (>95%, Sigma–Aldrich, 724769) were used to prepare $LiFeTiO_4$-carbon nanotube nanocomposites. 1 g of a mixture of the obtained $LiFeTiO_4$ powder and MWCNTs with a weight ratio of $LiFeTiO_4$ to MWCNTs of 4:1 was dispersed in 10 mL of ethanol, sonicated for 0.5 h and dried at room temperature. The dried sample was ball milled in the same magneto-ball mill for 12h at room temperature under Ar atmosphere (100 kPa). Rotation speed of 75 rpm was used and an external magnet removed in this preparation routine. Such a milling mode provides low-energy conditions suitable for preventing dramatic modification or damaging of ingredients during milling. A similar procedure of low-energy ball milling was described in detail elsewhere [22].

2.2. Characterization: X-ray diffraction (XRD) patterns of the samples were recorded on a PANalytical X'Pert PRO diffraction system using Cu X-ray source (λ = 1.5418 Å). Rietveld refinement was carried out in DIFFRACplus TOPAS 4.2 software using the fundamental parameters approach [23, 24]. The refinement was performed between 15-100° using a 5-parameter Chebyshev polynomial equation to fit the background. During refinements, only the position of O ions were refined and constrained to be equal to each other in terms of x, y and z to comply with cubic-close packing. The occupation factors of Li and Fe were also refined while those of Ti and O were kept constant at 0.5 and 1.0. The thermal parameters of all ions were kept at 0.5 since their refinements led to substantially larger errors.

Scanning electron microscopy (SEM, Carl Zeiss SUPRA55VP electron microscope) and transmission electron microscopy (TEM, JEOL JEM-2100F instrument operating at 200 kV) were used to investigate the structure, size, and morphology of the samples. Energy-filtered TEM (EFTEM) elemental maps were obtained using a Gatan Quantum ER 965 Imaging Filter installed on the JEOL JEM-2100F instrument. The three window method was used for the acquisition of the elemental maps. The Branauer-Emmett-Teller (BET) surface area of the sample was determined using a Micromeritics Tristar 3000 adsorption instrument. Thermal gravimetric analysis (TGA, Q50-1534 instrument, air flow, 20 °C/min heating rate) was used to estimate the carbon content in the sample.

2.3. Electrochemical experiments: Electrochemical measurements were performed using two-electrode coin cells (CR2032-type) assembled in an argon-filled glove box (Innovative Technology, USA). Li foil was used as a counter/reference electrode and a porous polyethene film was used as a separator. The electrolyte was 1 M $LiPF_6$ in a 1:1:1 (by volume) mixture of ethylene carbonate (EC), diethylene carbonate (DEC) and dimethyl carbonate (DMC). The slurry for the $LiFeTiO_4$ electrodes was prepared by mixing $LiFeTiO_4$ nanoparticles, carbon black, and polyvinylidene difluoride (PVDF) with a weight ratio of 75:15:10 in N-methylpyrrolidone (NMP) was coated on Al foils. The slurry for the $LiFeTiO_4$–carbon nanotube electrodes was prepared by mixing the active material ($LiFeTiO_4$–carbon nanotube composite) with carbon black and PVDF binder in a weight ratio of 80:10:10 in NMP. The slurry in each case was uniformly pasted on Al foils and the electrodes were dried in a vacuum oven at 100 °C for over 12 h. The electrochemical tests were performed using an Ivium-n-stat instrument (Ivium Technologies, the Netherlands) and LAND battery systems for charge-discharge (Wuhan Land Electronic Co. Ltd., China). The cells were galvanostatically discharged and charged over a voltage range of 1.5–4.5 V vs. Li/Li^+ at various current rates. Cyclic voltammetry (CV) experiments were performed over the same voltage range. Electrochemical impedance spectroscopy was performed in the frequency range between 100 kHz and 0.01 Hz at the level of the open circuit potential with amplitude of 5 mV. The capacity of the composite electrode was calculated for the total weight of the $LiFeTiO_4$ phase and MWCNTs.

3. Results and discussion

The SEM and powder XRD techniques were used for the assessment of the general morphology of the $LiFeTiO_4$-carbon nanocomposite as well as for the verification of the oxide phase in the as-produced nanoparticles and after their incorporation into the composite. An SEM image presenting the morphology of the $LiFeTiO_4$-carbon nanocomposite is shown in Figure 1a,b. Nanoscale particles as well as fibrous structures with typical diameters of 10-15 nm are visible. It is consistent with the idea that the $LiFeTiO_4$ component is embedded into a network of carbon nanotubes. As it is shown in the subsequent parts of the manuscript, such a structure of the nanocomposite is of critical importance for the significant improvement of the capacity and rate performance of the principal electrode component with a limited electronic conductivity. Powder XRD patterns of the as-obtained $LiFeTiO_4$ nanoparticles and the $LiFeTiO_4$-carbon nanocomposite are shown in Figure 1c. All significant peaks in both patterns can be indexed to the cubic $LiFeTiO_4$ (JCPDS No. 01-055-0988), indicating a reasonable phase purity of the $LiFeTiO_4$ nanoparticles not only in the original sample but also after embedding them into the network of carbon nanotubes by the low-energy mechanical milling.

A longer XRD scan was conducted to collect data suitable for Rietveld refinement. Figure 2a shows Rietveld refinement plot of $LiFeTiO_4$ which contains minor phase impurities, most probably due to Li_2O_3Ti (JCPDS No. 98-016-2215) and Fe_3O_4 (JCPDS No. 00-003-0863**)**. Except for the peaks from impurities, the refinements converged into a reasonably low reliability factor (R_{wp}) of 3.05, indicating a good fit. $LiFeTiO_4$ exhibits spinel structure with intermixed Li and Fe cations due to their almost similar size [25]. Rietveld refinement was performed to obtain the approximate distribution of Li and Fe in the tetrahedral sites (8a) and octahedral sites (16a) (Figure 2b and Table 1) of which Li occupies around 34% of the octahedral sites while Fe occupies around 56% of the tetrahedral sites, leading to a formula of

$(Li_{0.44}Fe_{0.56})(Li_{0.68}Fe_{0.32}Ti)O_4$. This implies a larger amount of Li in octahedral site and overall, a formation of a non-stoichiometric compound with a slight excess of Li (relative to Fe) – compare with the ideal stoichiometric formula of $(Li_{0.5}Fe_{0.5})(Li_{0.5}Fe_{0.5}Ti)O_4$.

Table 1. Lattice and atomic parameters of $LiFeTiO_4$ from Rietveld refinements

$LiFeTiO_4$						
Space group		Fd-3m				
Space group No.		227				
a (Å)		8.356(4)				
Atom	N_p	x	y	z	Occ.	b_{iso} (Å^2)
Ti	16	0.5	0.5	0.5	0.5	0.5
Li	16	0.5	0.5	0.5	0.34(1)	0.5
Fe	16	0.5	0.5	0.5	0.16(1)	0.5
Li	8	0.125	0.125	0.125	0.44(7)	0.5
Fe	8	0.125	0.125	0.125	0.56(7)	0.5
O	32	0.2514(5)	0.2514(5)	0.2514(5)	1	0.5
χ^2		1.41				
R_p (%)		2.31				
R_{wp} (%)		3.05				
R_{exp} (%)		2.17				
R_{Bragg} (%)		0.95				

The measured BET surface area of the $LiFeTiO_4$-carbon nanocomposite was 58.3 m^2 g^{-1}. Figure 3 shows the plot of the adsorbed amount vs. pressure points used for the calculation of BET area.

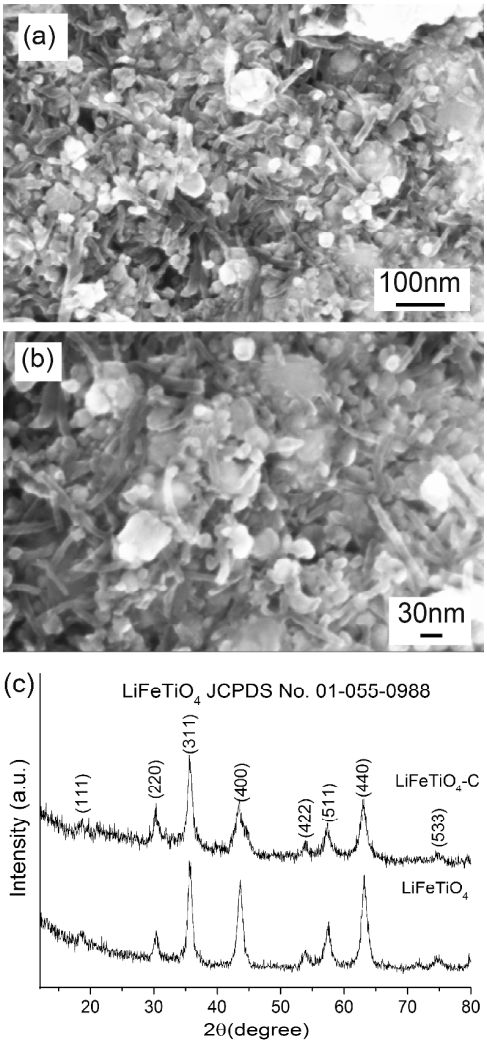

Fig.1. SEM images of $LiFeTiO_4$-carbon nanocomposite (a, b) and XRD patterns of $LiFeTiO_4$ nanoparticles and $LiFeTiO_4$-carbon nanocomposites (c).

The TEM characterisation further confirms these findings. Indeed, a bright-field image shown in Figure 4a displays a mixture of metal oxide particles (possessing a typical darker contrast) and MWCNTs. A selected area electron diffraction pattern (Figure 4b) includes a number of rings, consistent with the presence of a polycrystalline structure or a large number of randomly oriented nanoparticles. The pattern can be indexed in line with the diffraction rings of the $LiFeTiO_4$ phase, which correlates well with the XRD data. The crystallographic Miller indices corresponding to the visible rings in the electron diffraction pattern are labelled in Figure 4b.

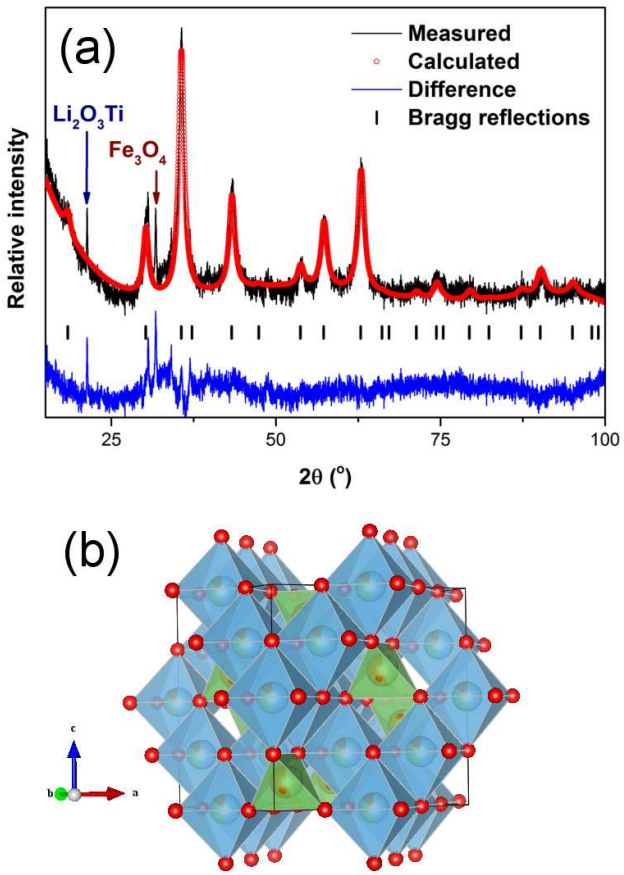

Fig. 2. Rietveld refinement of the crystal structure: (a) refinement plot of $LiFeTiO_4$ between 15-100°, (b) Structure of $LiFeTiO_4$ (drawn using VESTA) [26].

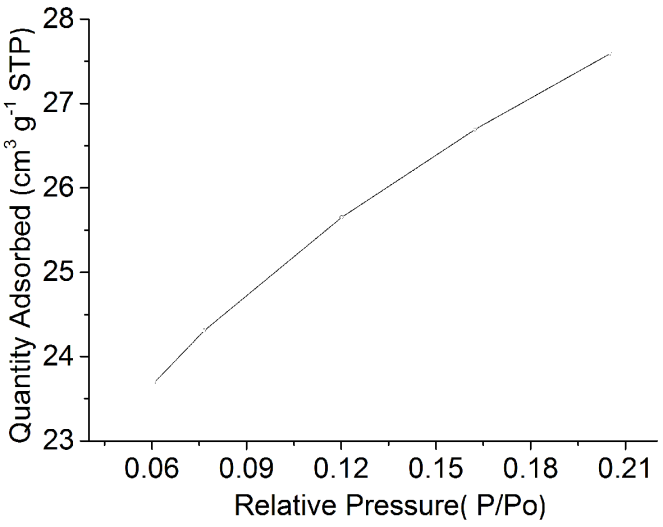

Fig. 3. The plot of the adsorbed amount vs. pressure points used for the calculation of BET surface area.

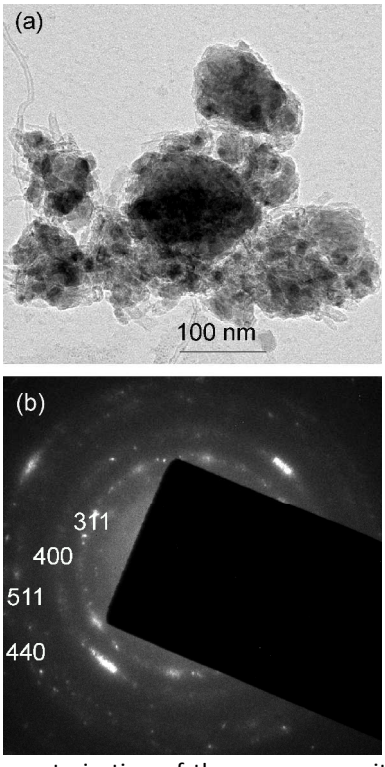

Fig.4. TEM characterisation of the nanocomposite: (a) bright-field image; (b) selected area diffraction pattern.

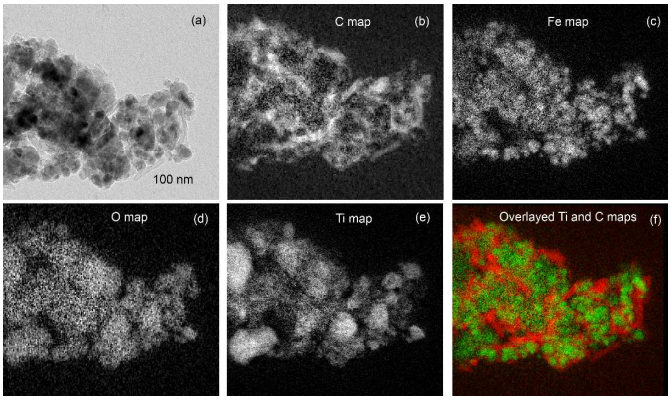

Fig.5. EFTEM analysis of the nanocomposite: (a) unfiltered bright-field image; (b, c, d, e) elemental maps of carbon, iron, oxygen and titanium; (f) an overlay of the titanium and carbon maps (colour scheme: Ti – green, C - red).

Energy-filtered TEM was employed to demonstrate the degree of mixing of $LiFeTiO_4$ particles and MWCNTs directly. A bright-field image is shown in Figure 5a and it displays rather confusing contrast due to the overlap between various components of the composite. Extracting chemical information via the filtering of electron energy helps to visualise the location of $LiFeTiO_4$ material and carbon nanotubes in the sample. Individual elemental maps of carbon, iron oxygen and titanium are shown in Figure 5(b, c, d, e). For obvious reasons, the Fe, O and Ti maps show similar distributions of these elements. One of the maps (Ti) was selected and plotted together with the carbon map in a colour-coded plot (Figure 5f). The overlay of the Ti and carbon maps (Figure 5f) displays the chemical information required for the correct interpretation of the bright-field image in Figure 5a and provides direct visualisation of the location of MWCNTs and $LiFeTiO_4$ nanoparticles in the sample. $LiFeTiO_4$ and CNT components are well-mixed in the nanocomposite. We believe that the $LiFeTiO_4$ particles are simply connected to each other via mechanical force. As it follows from TEM images (Figure 4 and 5), the sample represents aggregates of inorganic nanoparticles with nanotubes in which the network of nanotubes squeeze particles between individual nanotubes. It is also possible that some nanoparticles of $LiFeTiO_4$ may become cold welded to each other, as it is a well-known phenomenon in ball milling.

Figure 6 shows the TGA plot of the $LiFeTiO_4$-MWCNT composite in air. The low temperature weight loss (25-300 ^oC) is related to the departure of moisture and other adsorbed species as well as processes in the impurities present in the sample (<5 wt.%, according to the specification of MWCNTs). It is reasonable to attribute weight loss above 300 ^oC to the oxidation of nanotubes. Indeed, as Hsieh *et al.* [27] have shown by differential scanning calorimetry, the onset of the oxidation for the multiwalled carbon nanotubes is above 300 ^oC. We therefore attribute weight changes above 300 ^oC predominantly to the oxidation of carbon nanotubes. According to Figure 6, the weight loss between 300 and 500 ^oC is approximately 17.5 wt.% while 69.5 wt.% of the sample remains intact above 500 ^oC. We can estimate from this measurement that the weight ratio of $LiFeTiO_4$ to MWCNTs in the produced sample is likely to be about 3.97:1, close to the ratio of 4:1 between the initial ingredients for the preparation of the composite.

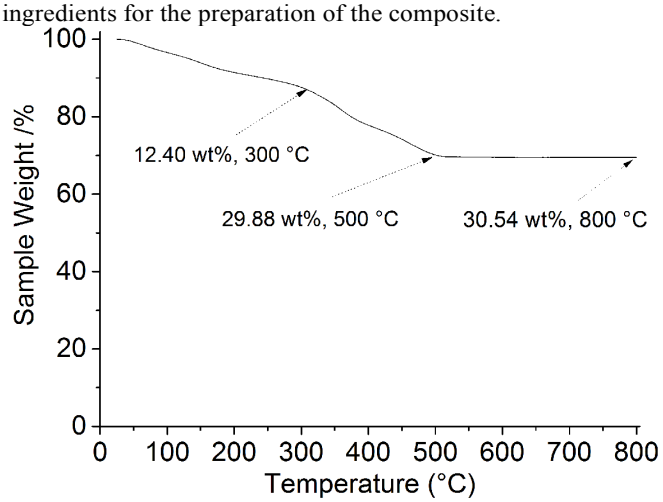

Fig. 6. TGA plot of the $LiFeTiO_4$-MWCNT composite in air.

Figure 7a shows the discharge capacities versus cycle number for $LiFeTiO_4$ and the $LiFeTiO_4$-MWCNT composite at a current rate of 25 mA g^{-1}. The $LiFeTiO_4$-C nanocomposite exhibits a stable discharge capacity of about 110 mAh g^{-1} after 100^{th} cycles, which is much higher than that of $LiFeTiO_4$ nanoparticles (about 70 mAh g^{-1}). The Coulombic efficiencies of the two electrodes are also plotted in the same graph. The corresponding selected discharge-charge voltage profiles for the nanocomposite electrode from the first 50 cycles are shown in Figure 7b. The shape of the profiles does not change significantly during cycling, indicating good capacity retention at slow current rates. The rate capabilities of both the $LiFeTiO_4$ and $LiFeTiO_4$-MWCNT electrodes were tested at various current densities between 12.5 and 500 mA g^{-1} (Figure 7c, d). It is apparent that the capacity retention for the composite electrode is superior, and the discharge capacities of 135, 122, 112, 97, 76, and 65 mA h g^{-1} were recorded for this electrode after 20 cycles at current densities of 12.5, 25, 50, 100, 200, and 500 mA g^{-1}, respectively. The composite electrode can obviously operate at up to 500 mA g^{-1} currents and retain capacity equal to or above that of $LiFeTiO_4$ nanoparticles at a slow current rate of 25 mA g^{-1}.

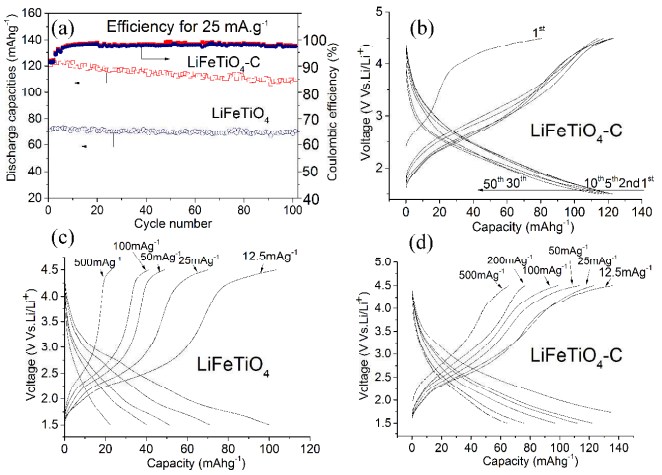

Fig.7. Discharge capacity vs. cycle number for the $LiFeTiO_4$-carbon nanocomposite and $LiFeTiO_4$ nanoparticles (a), selected galvanostatic charge/discharge curves at 25 mA g^{-1} for the

$LiFeTiO_4$-carbon nanocomposite (b), and charge–discharge voltage profiles for the $LiFeTiO_4$ electrode (c) and nanocomposite in the 20th cycle at various current rates (d).

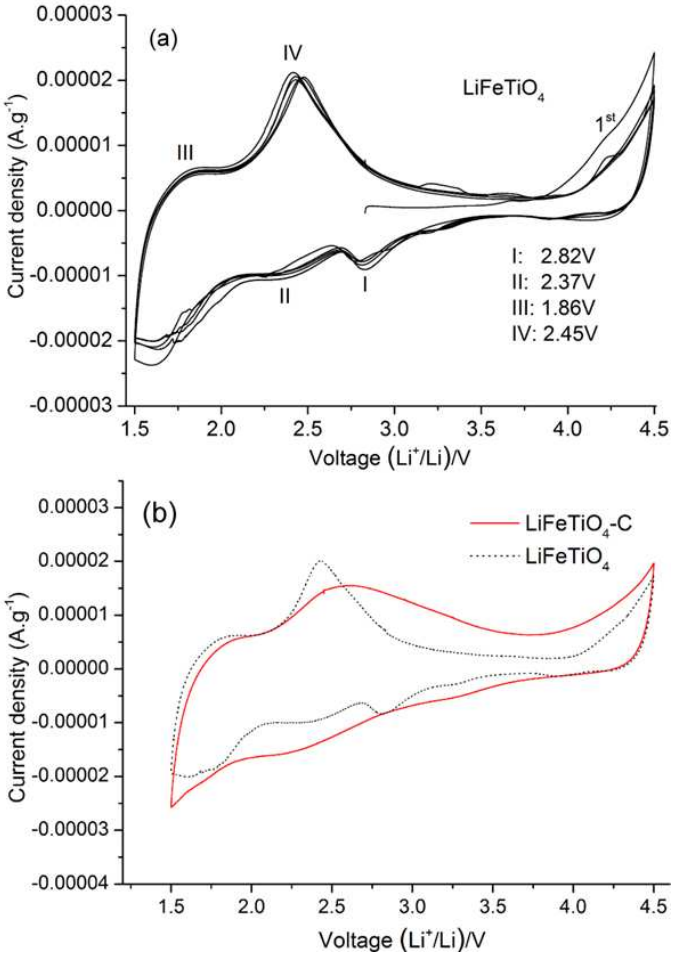

Fig. 8. Typical cyclic voltammograms: the first and subsequent cycles of the $LiFeTiO_4$ electrode (a), and comparison of the electrode assembled with the $LiFeTiO_4$-carbon nanocomposites and $LiFeTiO_4$ nanoparticles (b). The CV measurements were performed at a scan rate of 0.2 mV s^{-1} in the voltage range of 1.5–4.5 V vs. Li/Li^+.

It is important to note that the capacity of the $LiFeTiO_4$ and $LiFeTiO_4$-MWCNT electrodes depends on the chosen potential range and will be smaller if the potential range of 2.0 – 4.5 is used. To complete the electrochemical characterisation, we have also included the CV curves for $LiFeTiO_4$ and $LiFeTiO_4$-MWCNT electrodes here (Figure 8).

Electrochemical impedance spectroscopy measurements were carried out for the assembled cells (open circuit potential state) to investigate the rate of electron transfer in the $LiFeTiO_4$ and $LiFeTiO_4$-MWCNT electrodes. Typical Nyquist plots recorded for both electrodes are presented in Figure 9. Both plots display one compressed semicircle in the high to medium frequency region and a sloped line in the low-frequency region. The diameter of each semicircle is related to the charge transfer resistance (R_{ct}). The smaller the diameter, the smaller the charge transfer resistance is, and this parameter is a function of the electronic conductivity in the electrodes [28, 29]. It is clearly observed that diameter of the composite $LiFeTiO_4$-MWCNT electrode is much smaller than that of the $LiFeTiO_4$-based electrode. The values of R_{ct} for the $LiFeTiO_4$ and $LiFeTiO_4$-MWCNT electrodes were calculated to be 829 Ω and 199 Ω, respectively. This indicates that $LiFeTiO_4$ particles mixed with carbon nanotubes in a composite provide much easier charge transfer at the electrode/electrolyte interface, and that consequently decreases the overall battery internal resistance, enabling higher reactivity and lower polarisation [30, 31]. The underlying reason is the significant enhancement of the electronic conductivity in the electrode based on the $LiFeTiO_4$-MWCNT composite; the nanotubes provide conductive paths in the vicinity of the $LiFeTiO_4$ nanoparticles, and this is a key factor in improving the discharge capacity and rate capability of the $LiFeTiO_4$-MWCNT electrode in respect to those of a more conventional $LiFeTiO_4$ electrode.

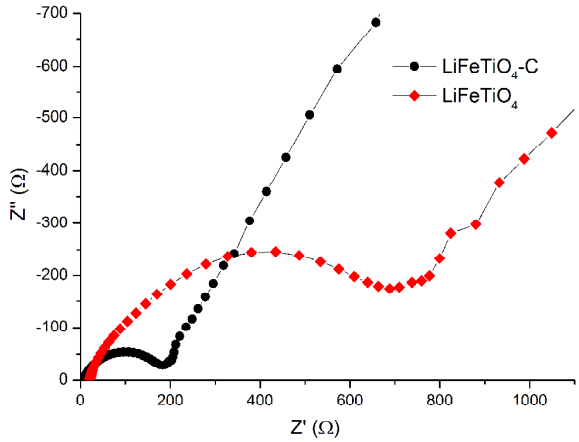

Fig.9. Electrochemical impedance spectra for the assembled coin cells incorporating working electrodes based on $LiFeTiO_4$ nanoparticles and the $LiFeTiO_4$-MWCNT composite.

4. Conclusions

We have demonstrated a simple method to prepare nanocomposites of oxide phases with carbon nanotubes. The method is based in low-energy ball milling. Using an insulating phase of $LiFeTiO_4$ as a test electrode material, we have shown that the $LiFeTiO_4$ - MWCNT nanocomposite displays capacity significantly higher than that of $LiFeTiO_4$ nanoparticles (105-120 mAh g^{-1} vs. 65-70 mAh g^{-1} at a slow current rate of 25 mA g^{-1}). The composite electrode can also operate at relatively high currents (current rates of up to 500 mA g^{-1} were evaluated). Transmission electron microscopy shows that good intimate mixing between $LiFeTiO_4$ particles and carbon nanotubes has been achieved. That results in the dramatically improved electronic conductivity of the nanocomposite electrode, which agrees with the results of the impedance spectroscopy measurements.

Acknowledgements
Financial support from the Australian Research Council is acknowledged. The authors also thank technical officers at Deakin University for their help in this work and acknowledge the use of electron microscopes in the Victorian Node of the Australian National Fabrication Facility (ANFF).

Notes and references

[a] Institute for Frontier Materials, GTP, Deakin University, Geelong Waurn Ponds Campus, Locked Bag 20000, Geelong, VIC 3220, Australia
[b]Department of Chemistry, University of Waterloo, 200 University Avenue West, Waterloo, ON N2L 3G1, Canada
[c] Melbourne Centre for Nanofabrication, 151 Wellington Rd, Clayton, VIC 3168, Australia

References

1 V. Etacheri, R. Marom, R. Elazari, G. Salitra and D. Aurbach, *Energy Environ. Sci.*, 2011, **4**, 3243.
2 R. Marom, S. F. Amalraj, N. Leifer, D. Jacob and D. Aurbach, *J. Mater. Chem*., 2011, **21**, 9938.
3 A. Manthiram, *J. Phys. Chem. Lett.* 2011, **2**, 176.
4 A. K. Padhi, K. S. Nanjundaswamy and J. B. Goodenough, *J. Electrochem. Soc.,* 1997, **144**, 1188.
5 B. L. Ellis , K.T. Lee and L. F. Nazar, *Chem. Mater.,* 2010, **22**, 691–714.
6 K. Zaghib, M. Dontigny, A. Guerfi, P. Charest, I. Rodrigues, A. Mauger and C. M. Julien, *J. Power Sources,* 2011, **196**, 3949–3954.
7 N. Ravet, Y. Chouinard, J.F. Magnan, S. Besner, M. Gauthier and M. Armand, *J. Power Sources*, 2001, **97-98**,503.
8 H. Q. Li and H. S. Zhou, *Chem. Commun.* 2012, **48**, 1201.
9 C. de las Casas and W. Z. Li, *J. Power Sources*, 2012, **208**, 74.
10 L. M. Dai, D. W. Chang and J. B. Ba, *Small*, 2012, **8**,1130.
11 X. M. Liu, Z. D. Huang, S. W. Oh, B. Zhang, P. C. Ma, M. M. F. Yuen and J. K. Kim, *Compos Sci Technol.,* 2012, **72**, 121.
12 S. B. Ma, K. W. Nam, W. S. Yoon, S. M. Bak, X. Q. Yang, B. W. Cho and K. B. Kim, *Electrochem Commun,* 2009, **11**, 1575.
13 G. X. Wang, X. P. Shen, J. Yao, D. Wexler and J. H Ahn, *Electrochem Commun.,* 2009, **11**, 546.
14 C. M. Ban, Z. Li, Z. C. Wu, M. J. Kirkham, L. Chen, Y. S. Jung, E. A. Payzant, Y. F. Yan, M. S. Whittingham and A. C. Dillon, *Adv. Energy Mater*., 2011, **1**, 58.
15 A. L. M. Reddy, M. M. Shaijumon, S. R. Gowda and P. M. Ajayan, *Nano Lett.*, 2009, **9**, 1002.
16 S. J. Ding, J.S. Chen, X. W. Lou, *Adv. Funct. Mater.*, 2011, **21**, 4120.
17 S. R. Bruno, C. K. Blakely and V.V. Poltavets, *ECS Transactions*, 2012, **41** (29), 29.
18 S. R. Bruno, C. K. Blakely and V. V. Poltavets, Abstract #214, 221st ECS Meeting, © 2012 *The Electrochemical Society*.
19 S. Chakrabarti, A. K. Thakur and K. Biswas, *Solid State Ionics*, 2014, 262, 49.
20 S. R. Bruno, C. K. Blakely and V. V. Poltavets, *ECS Transactions*, 2013, **45** (29), 23.
21 T. Tao, A.M. Glushenkov, H.W. Liu, Z.W. Liu, X.J. Dai, H. Chen, S.P. Ringer and Y. Chen, *J. Phys. Chem. C,* 2011, **115**,17297.
22 T. Tao, A. M. Glushenkov, C. Zhang, H. Zhang, D. Zhou, Z. Guo, H. K. Liu, Q. Chen, H. Hu and Y. Chen, *J. Mater. Chem,.* 2011, **21**, 9350.
23 A. Coelho, Bruker AXS GmbH, Karlsruhe, Germany 2008
24 R. W. Cheary, A. Coelho, *J. Appl. Cryst.,* 1992, **25**, 109.
25 M. A. Arillo, M.L. López, E. Perez-Cappe, C. Pico, M.L. Veiga, *Solid State Ionics,* 1998, **107**, 307.
26 K. Momma, F. Izumi, Visualization for Electronic and Structural Analysis Ver.3.1.0. Copyright © 2006-2012.
27 Y. C. Hsieh, Y.C. Chou, C.P. Lin, T.F. Hsieh, C.M. Shi, *Aerosol and Air Quality Research*, 2010, **10**, 212.
28 L. F. Jiao, H. T. Yuan, Y. C. Si, Y. J. Wang and Y. M. Wang, *Electrochem. Commun.,* 2006, 8, 1041.
29 Y. Shao, M. Engelhard andY. Lin, *Electrochem. Commun.*, 2009, 11, 2064.
30 M.M. Rahman, J.Z. Wang, M.F. Hassan, S. Chou, Z.X. Chen and H.K. Liu, *Energy Environ. Sci.,* 2011, 4, 952.
31 M.F. Hassan, M.M. Rahman, Z. Guo, Z. Chen and H.K. Liu, *J. Mater. Chem.,* 2010, 20, 9707.